Mon. Not. R. Astron. Soc. **000**, 1–9 (2012) Printed 3 March 2013 (MN LaTeX style file v2.2)

arXiv:1204.5816v1 [astro-ph.GA] 26 Apr 2012

# Discovery of Multiple Shells Around the Planetary Nebula IC 418

G. Ramos-Larios[1]⋆ R. Vázquez[2], M.A. Guerrero[3], L. Olguín[4], R.A. Marquez-Lugo[1] and H. Bravo-Alfaro[5]

[1] *Instituto de Astronomía y Meteorología, Av. Vallarta No. 2602, Col. Arcos Vallarta, C.P. 44130 Guadalajara, Jalisco, Mexico.*
[2] *Instituto de Astronomía, Universidad Nacional Autónoma de México, Apdo. Postal 877, 22800 Ensenada, B.C., Mexico*
[3] *Instituto de Astrofísica de Andalucía, IAA-CSIC, C/ Glorieta de la Astronomía s/n, 18008 Granada, Spain*
[4] *Dpto. de Investigación en Física, Universidad de Sonora, Blvd. Rosales-Colosio, Ed. 3H, 83190, Hermosillo, Sonora, Mexico*
[5] *Departamento de Astronomía, Universidad de Guanajuato, Apdo. Postal 144, Guanajuato 36000, Mexico*

Received 2011 September 27; in original form 2011 June 16

## ABSTRACT

We have analysed optical, near-, and mid-IR images of the bright planetary nebula (PN) IC 418. These images probe unambiguously for the first time a number of low surface brightness structures and shells around the bright main nebula, including radial filaments or rays, a system of three concentric rings, and two detached haloes with sizes $\sim 150''$ and $220''\times 250''$, respectively. The main nebula is slightly off-centered with respect to the elliptical outer halo. The time-lapse between the two haloes is 10,000–50,000 yr, whereas the time-lapse between the three concentric rings is $\sim$630 yr. We emphasize the advantages of near- and mid-IR imaging for the detection of faint structures and shells around optically bright nebulae.

**Key words:** (ISM:) planetary nebulae: individual: IC 418 — ISM: jets and outflows — infrared: ISM — ISM: lines and bands

## 1 INTRODUCTION

IC 418 is a bright elliptical planetary nebula (PN) whose physical structure and emission properties have been subject of numerous observational studies and theoretical modeling (e.g., Phillips, Riera, & Mampaso 1990b; Zhang & Kwok 1992; Hyung, Aller, & Feibelman 1994; Meixner et al. 1996; Morisset & Georgiev 2009). The nebula is described as a high density ellipsoidal shell with chemical abundances typical of type II PNe. The distance to IC 418 is 1.3±0.4 kpc as determined from VLA parallax expansion observations spanning more than 20 years in time (Guzmán et al. 2009), making of IC 418 one of the few PNe with a reliable distance measurement. Its central star has a relatively low effective temperature of 39,000 K (Pottasch et al. 2004), and a surface gravity $\log(g)$ of 3.70 (Pauldrach, Hoffmann, & Méndez 2004), implying an early evolutionary stage.

Whereas the overall morphology of IC 418 seems simple, the detailed view of this bright nebula offered by *HST* WFPC2 images (Sahai & Trauger 1998) reveals an intricate cyclic pattern that has dubbed it as the "Spirograph Nebula". The origin of this complex pattern is intriguing: magnetic fields have been claimed to be responsible for these structures (Huggins & Manley 2005), although the action of its variable stellar wind, revealed by changes in the P Cygni profiles of high excitation lines detected by *FUSE* (Prinja et al. 2012, Guerrero & De Marco, in preparation) and the photometric variability of the central star (Handler et al. 1997), can also be linked to the formation of this singular pattern.

The Zanstra temperatures of IC 418 have been reported to be $T_{\rm Z}$(H I) = 38,000 K and $T_{\rm Z}$(He II) = 44,000 K (e.g., Phillips 2003), which are in agreement with the temperature estimate obtained from the energy balance method (Pottasch et al. 2004). A small difference between the H I and He II Zanstra temperatures is traditionally interpreted as proof of the large optical thickness of the nebula to H-ionising radiation. Therefore, significant amounts of atomic and molecular material, as well as dust, may survive outside the ionisation bound optical nebula.

Detached low surface brightness shells, i.e., haloes, are typically found around PNe (e.g., Chu, Jacoby, & Arendt 1987). These haloes have been associated to the final mass-loss episodes that occur in the late phases of the AGB (Balick et al. 1992), and therefore they can provide information on the late AGB evolution (e.g., Frank, van der Veen, & Balick 1994; Stanghellini & Pasquali 1995; Hajian et al. 1997). The

---

⋆ E-mail: gerardo@astro.iam.udg.mx (GRL)

**Table 1.** NIR Imaging of IC 418

| Telescope | Filter | $\lambda_c$ ($\mu$m) | $\Delta\lambda$ ($\mu$m) | Exp. Time (s) |
|---|---|---|---|---|
| 2.1m OAN-SPM | J | 1.275 | 0.282 | 600 |
| 2.1m OAN-SPM | H | 1.672 | 0.274 | 400 |
| 2.1m OAN-SPM | K' | 2.124 | 0.337 | 300 |
| 3.5m TNG-ORM | J | 1.270 | 0.300 | 50 |

identification and detection of low surface brightness shells around bright PNe is hampered by light from the inner shell dispersed within the optical system used for the observations (see Corradi et al. 2003, for a thorough description of the observational problems associated to such studies).

An early investigation of IC 418 by Phillips et al. (1986) proposed that the unusually extended near-IR emission may arise from high temperature, small-sized dust grains. It was also proposed that scattering could result in a $\sim$40$''$ in diameter optical halo (e.g., Phillips, Riera, & Mampaso 1990a,b) The presence of this halo and the high temperature of the dust have been later confirmed by the analysis of $J-H$ and $H-K_s$ maps by Phillips & Ramos-Larios (2005) who also suggested that the grains are probably mixed with a dilute ionised gas. Recently, Morisset et al. (2012) have modelled the IR dust emission from 2 to 200 $\mu$m and concluded that the dust is carbon rich.

Meanwhile Monk, Barlow, & Clegg (1990) have argued that such outer shell is not real, but it should be attributed to a mix of Galactic background emission and extended King seeing function. On the other hand, Taylor, Gussie, & Goss (1989) detected a region of H I emission whose spatial extent seems to be coincident with the region described by Phillips, Riera, & Mampaso (1990b), whereas Gussie et al. (1995) found no evidence for molecular emission. These results suggest that the material outside the bright inner shell of IC 418 is photo-dissociated. Indeed, Meixner et al. (1996), using mid-IR and radio images, suggested that the inner shell of IC 418 is surrounded by a low density ionised region with radius $\sim$20$''$ that is enclosed into an atomic neutral halo with an outer radius of 90$''$. Additional evidence for the occurrence of a halo of ionised material is provided by the near-IR spectroscopy of this region reported by Hora, Latter, & Deutsch (1999) who detected emission in the Pa$\beta$ $\lambda$1.2817 $\mu$m, Br8 H I $\lambda$1.9446 $\mu$m, He I $\lambda$2.058 $\mu$m, and Br$\gamma$ $\lambda$2.1658 $\mu$m lines. Unfortunately, the exact location of the slit (east of the main nebula) and extent of the emission are not described, hence the nature of the outer shell mentioned by these authors and its spatial extent remains uncertain.

In order to assess the presence of material outside the bright ionised shell of IC 418 and to investigate its nature, we have acquired new broad-band deep near-IR *JHK* images, and long slit intermediate- and high-dispersion spectroscopic observations that have been examined in conjunction with archival mid-IR *WISE* images. The observations and archival data are presented in §2 and the results are described in §3. The discussion and final summary are presented in §4 and §5, respectively.

## 2 OBSERVATIONS AND ARCHIVAL DATA

### 2.1 Optical imaging

Narrow-band *HST* WFPC2 images of IC 418 in the H$\alpha$, [N II] $\lambda$6583, and [O III] $\lambda$5007 emission lines were retrieved from HLA, the Hubble Legacy Archive[1] at the Space Telescope Science Institute[2] (Prop. ID: 6353, PI: R. Sahai, and Prop. ID: 8773, PI: A. Hajian).

The 888 s H$\alpha$ image was obtained from eight individual exposures acquired through the F656N filter (pivot wavelength $\lambda_\mathrm{p}$=6563.8 Åand band-width $\Delta\lambda$=21.5 Å), whereas the 700 s [N II] image and the 600 s [O III] were obtained from three individual exposures acquired using the F658N ($\lambda_\mathrm{p}$=6590.8 Å, $\Delta\lambda$=28.5 Å) and F502N ($\lambda_\mathrm{p}$=5012.4 Å, $\Delta\lambda$=26.9 Å) filters, respectively.

### 2.2 Near-IR imaging

Broad-band near-IR images of IC 418 were acquired on October 23, 2005 using the CAMILA infrared camera (Cruz-González et al. 1994) mounted with f/4.5 focal reducing optics at the f/13.5 primary focus of the 2.1m telescope at the Observatorio Astronómico Nacional, San Pedro Mártir (OAN-SPM, Baja California, Mexico). CAMILA has a 256×256 pixel NICMOS3 detector with a plate scale of 0$''\!.$85 pixel$^{-1}$ and a field of view (FoV) of 3$'\!.$6×3$'\!.$6. Further details of the observations are provided in Table 1.

The source was observed following a typical on-off sequence and the resulting individual frames were reduced following standard procedures. The seeing was $\simeq$2$''\!.$6.

A broad-band $J$ image of the central source of IC 418 was also obtained on October 13, 2008 using NICS, the Near Infrared Camera Spectrometer (Baffa et al. 2001), at the Cassegrain focus of the 3.5-m Telescopio Nazionale Galileo (TNG) on Roque de Los Muchachos Observatory (ORM, La Palma, Spain). NICS is a multimode instrument for near-IR observations in the range 0.9–2.5 $\mu$m that employs a Rockwell 1024×1024 HgCdTe Hawaii array. The large field (LF) mode was used, providing a plate scale of 0$''\!.$25 pixel$^{-1}$ and a FoV of 4$'\!.$2×4$'\!.$2. Five 10 s exposures were secured for a total effective exposure time of 50 s (Table 1).

The NICS data reduction was carried out using SNAP (Speedy Near-IR data Automatic reduction Pipeline), a pipeline for the automatic reduction of near-IR data that uses pieces of existing software such as IRDR[3], IRAF[4], Sextractor, and Drizzle[5]. The reduction performed by SNAP includes additional non-standard steps such as cross-talk correction, double-pass sky subtraction, and field distortion correction. The spatial resolution, as determined from the FWHM of stars in the FoV, is $\simeq$0″.7.

---

[1] http://hla.stsci.edu/

[2] STScI is operated by the Association of Universities for Research in Astronomy, Inc., under NASA contract NAS5-26555.

[3] IRDR, the Infra-Red Data Reduction, is a C library and set of stand-alone C programs and perl scripts for processing IR imaging data that is distributed by the Institute of Astronomy (IoA), at the University of Cambridge.

[4] IRAF, the Image Reduction and Analysis Facility, is distributed by the National Optical Astronomy Observatory, which is operated by the Association of Universities for Research in Astronomy (AURA) under cooperative agreement with the National Science Foundation.

[5] Drizzle is available as an IRAF task as part of the Space Telescope Science Data Analysis System (STSDAS) package and can

### 2.3 Mid-IR imaging

Wide-field Infrared Survey Explorer, *WISE* (Wright et al. 2010), images of IC 418 were retrieved from the NASA/IPAC Infrared Science Archive (IRSA). *WISE* is a NASA Explorer mission that surveys the entire sky at 3.4, 4.6, 12, and 22 $\mu$m, the so-called W1 through W4 bands, with 5$\sigma$ point source sensitivities better than 0.08, 0.11, 1, and 6 mJy, respectively.

The 40-cm telescope uses HgCdTe and Si:As detectors arrays with a plate scale of 2″.75 pixel$^{-1}$. The data were downloaded from the *WISE* first data release that includes a preliminary catalogue of sources and an image atlas based on early data that covers more than 55% of the sky. The angular resolution in the four bands is 6″.1, 6″.4, 6″.5, and 12″.0, respectively, and the astrometric accuracy for bright sources is better than 0″.15.

### 2.4 Long-slit optical spectroscopy

Long-slit high dispersion optical spectroscopy of IC 418 was acquired on December 2010 and February 2011 using the Manchester Echelle Spectrometer (MES, Meaburn et al. 2003) at the f/7.5 focus of the OAN-SPM 2.1m telescope. Since the spectrometer has no cross-dispersion, a $\Delta\lambda$=90Å bandwidth filter was used to isolate the 87$^{\rm th}$ order of the spectrum covering the H$\alpha$ and [N II] $\lambda\lambda$6548,6583Å lines. The 2048 × 2048 Thomson CCD with a pixel size of 15$\mu$m was used, resulting a plate scale of 0″.352 pixel$^{-1}$ and a dispersion of 0.06 Å pixel$^{-1}$.

Two slits at PA=0° and PA=275°, crossing the central star, were taken with an exposure time of 120 s. The data were bias-substracted and wavelength calibrated using a ThAr lamp, with a precision in velocity of $\pm$1 km s$^{-1}$. The seeing during the observations, as determined from the FWHM of stars in the FoV, was 1″.0.

Low dispersion, long-slit optical spectra of IC 418 was obtained on two observational runs. The first on 2011 April 2, using the Boller & Chivens spectrometer mounted at the prime focus of the 2.1 m telescope at the Observatorio Astronómico Nacional, San Pedro Mártir, Baja California, Mexico. The Marconi 2048×2048 CCD was used as a detector, in conjunction with a 400 l mm$^{-1}$ grating blazed at 5500 Å. The slit had a length of 5′ and a width of 200 $\mu$m ($\equiv$2″). The plate and spectral scales were 0″.57 pixel$^{-1}$ and 1.7 Å pixel$^{-1}$, respectively. The spectral resolution was $\sim$4 Å, the wavelength uncertainty was $\sim$1 Å, and the spectral range covered was 4080–7560 Å. One 1800 s exposure was obtained with the slit oriented along the East-West direction and offset by 23″ North from the central star. The mean air mass during the observations was $\simeq$1.4. The observations were flux calibrated using a 600 s exposure of the star Hz 44 obtained with an airmass of 1.03 on the same night. The

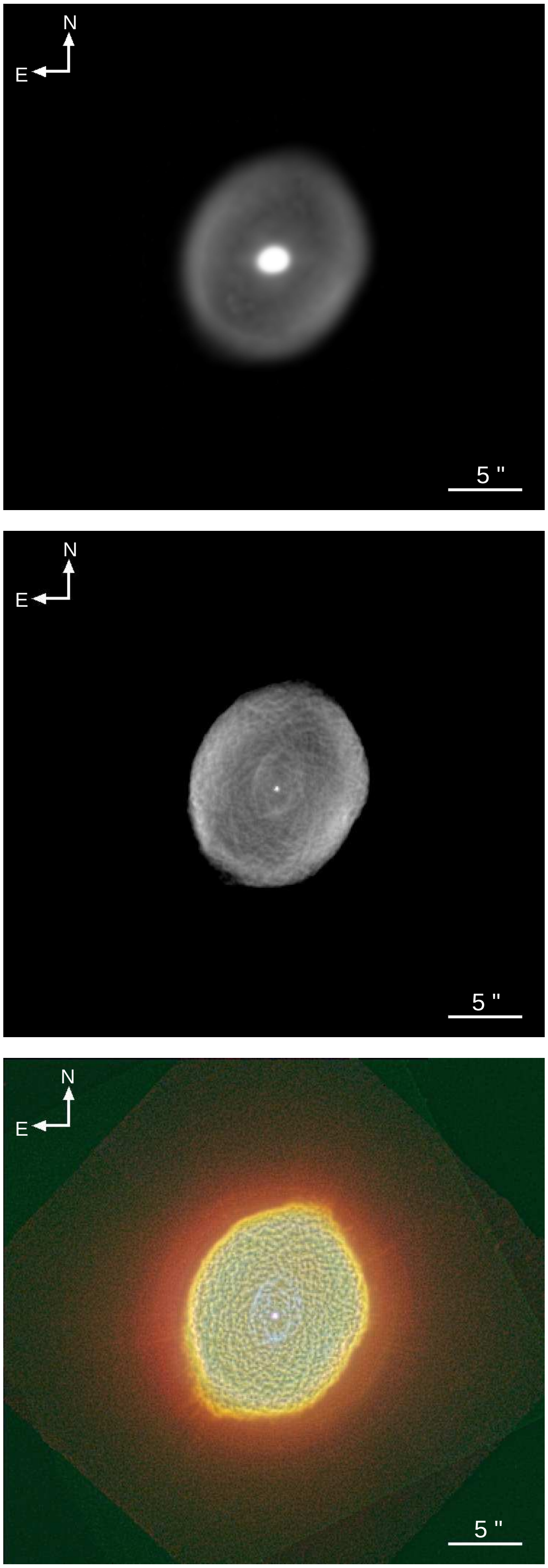

**Figure 1.** TNG *J (top)*, *HST* H$\alpha$ *(middle)*, and *HST* colour composite *(bottom)* pictures of IC 418. The *HST* colour composite picture has been processed using unsharp masking techniques and includes the [O III] $\lambda$5007 (blue), H$\alpha$ (green), and [N II] $\lambda$6583 (red) narrow-band images.

---

be retrieved from the Space Telescope Science Institute (STScI) web site.

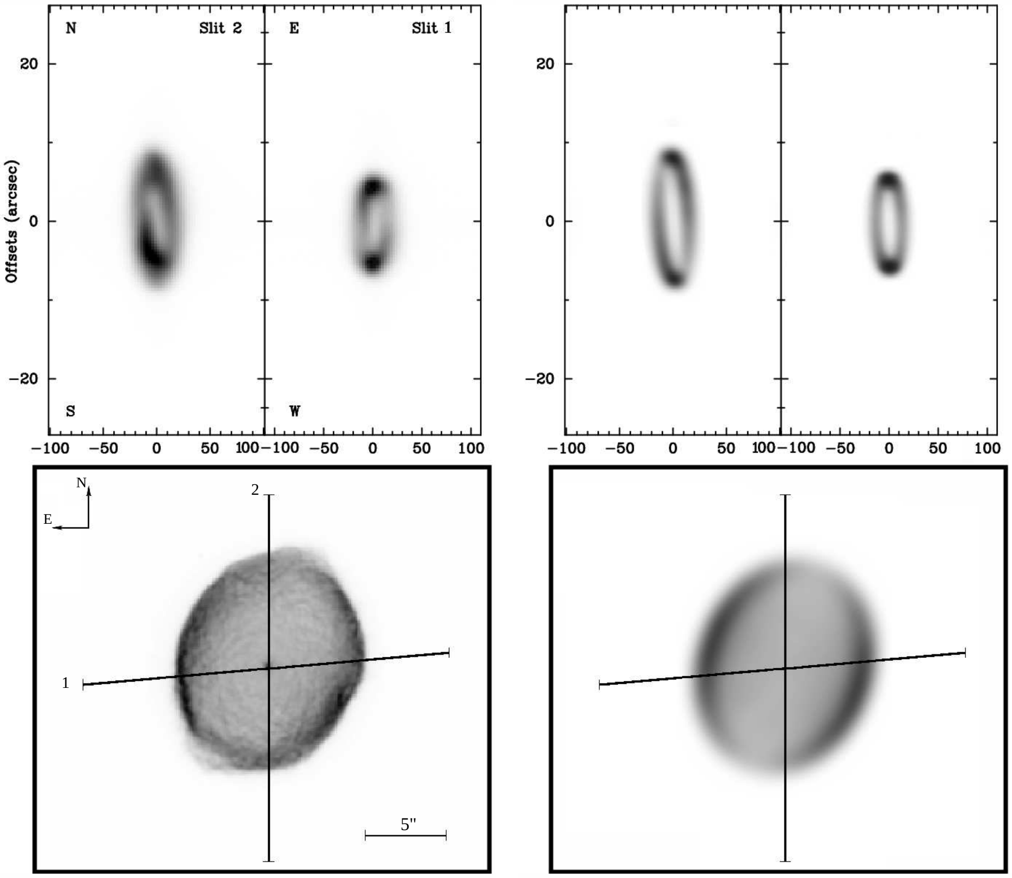

**Figure 2.** *Left* (*top*) Position-velocity (PV) maps of the inner shell of IC 418 and (*bottom*) *HST* WFPC2 [N II] image overplotted by the positions of the long-slits used for the Echelle spectroscopy. The slits orientation are labeled on the panels. *Right* (*top*) Synthetic SHAPE (PV) maps of the IC 418 core and (*bottom*) SHAPE model of IC 418.

seeing as determined from the FWHM of stars in the FoV, was ∼2.″5.

Additional low-dispersion spectra of IC 418 were obtained on 2011 October 4, using the Albireo spectrograph at the 1.5 m telescope of the Observatorio de Sierra Nevada (OSN), Granada, Spain. The Marconi 2048×2048 CCD was used in conjunction with a 400 l mm$^{-1}$ grating blazed at 5500 Å. The slit length was ∼6′ and its width was set at 50 $\mu$m (≡2.5″). The binning 2×2 of the detector implied plate and spectral scales of 0.″30 pix$^{-1}$ and 1.89 Å pix$^{-1}$, respectively. The spectral resolution was ∼4.7 Å, the wavelength-calibration uncertainty ∼1 Å, and the spectral range covered 3500–10000 Å. Two positions with exposures of 900 and 1800 seconds were obtained with the slit oriented along the North-South direction (P.A.=0°) and offset by 65″ and 105″ West from the central star, respectively. The observations were flux calibrated using spectra of the spectrophotometric standard star Hiltner 600 acquired on the same night. The seeing, as determined from the FWHM of stars in the FoV, was ∼2.″5.

All intermediate-dispersion spectra were bias-subtracted, flat-fielded, and wavelength and flux calibrated following standard procedures using XVISTA[6], IRAF and the nebular analysis software ANNEB (Olguín et al. 2011) which integrates the NEBULAR package of IRAF/STSDAS (Shaw & Dufour 1995).

## 3 MULTIPLE SHELLS AROUND IC 418

The new images of IC 418 reveal a wealth of structures around its ionised bright shell. These are described into further detail below.

### 3.1 The inner shell

Detailed morphological descriptions of the inner shell of IC 418 abound in the literature (see, for instance, the recent work by Sahai, Morris, & Villar 2011, and references therein). We will mention here the distinctive pattern of interwound features (Figure 1-*bottom*), and the 3.″5×5.″5 shell interior to the 11″×14″outer shell. This inner shell is particularly bright in [O III], fainter in H$\alpha$, and undetected in [N II], implying a higher relative excitation, a

---

[6] XVISTA is maintained and distributed by Jon Holtzman at the New Mexico State University http://astro.nmsu.edu/∼holtz/vista

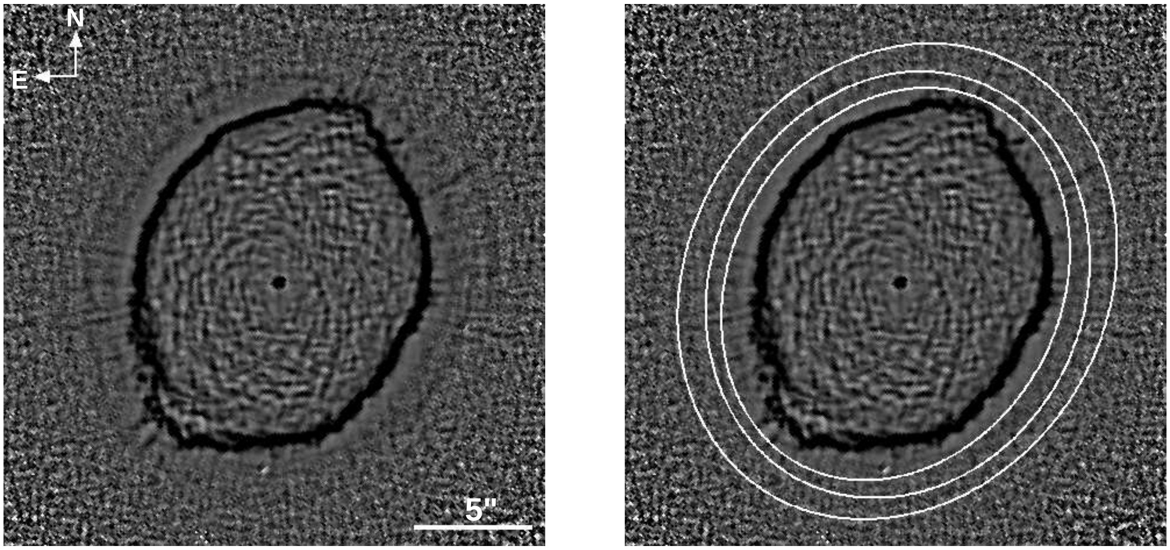

**Figure 3.** *HST* [N II] image of IC 418 processed to emphasize the ring features around the bright inner shell following the techniques developed by Corradi et al. (2004). This process has also enhanced a series of radial filaments in the image. The left panel corresponds to the processed image, where darker shades of grey indicate higher levels of emission. The location of the rings has been overlaid by white arcs in the right panel.

characteristic which is common of other PNe with these inner bubbles (Sahai, Morris, & Villar 2011). Finally, we note the morphological similarities between the H$\alpha$ and near-IR $J$ images (Figure 1-*top,middle*) which suggests that the $J$ band image is dominated by the H I Pa$\beta$ $\lambda$1.2817 $\mu$m line (Hora, Latter, & Deutsch 1999).

It is noticeable that, in spite of the high brightness of IC 418 and the substantial number of studies in the literature about its morphology and physical conditions, a spatio-kinematical study of its three-dimensional structure is lacking. We next describe a simple morpho-kinematical model that fits the observations described in §2.

Figure 2 (*bottom-left*) presents the *HST* image of the inner shell overplotted with the two slits going across the central star. The corresponding [N II] PV maps of the inner shell are presented in Figure 2 (*top-left*). We have used the computational tool SHAPE (Steffen et al. 2011) to construct a simple 3D model of IC 418 by fitting simultaneously the [N II] *HST* image (morphology) and PV maps (kinematics). The best model consists of an ellipsoid with semi-major axis of 6.″6 and semi-minor axis of 5.″3 oriented along PA= 341° and with an inclination angle of $i = 65°$ with respect to the line of sight. Assuming homologous expansion, we derive a polar velocity $V_{\rm pol} = 15.7$ km s$^{-1}$ and an equatorial velocity $V_{\rm eq} = 12.6$ km s$^{-1}$, notably larger than the expansion velocity of 5 km s$^{-1}$ recently reported by Jacob et al. (2012), but consistent with the value of 12 km s$^{-1}$ provided by Gesicki, Acker, & Szczerba (1996). The kinematical age of the model, for the distance of 1.3 kpc, is $\tau_{\rm kin} = 2600 \pm 800$ yr.

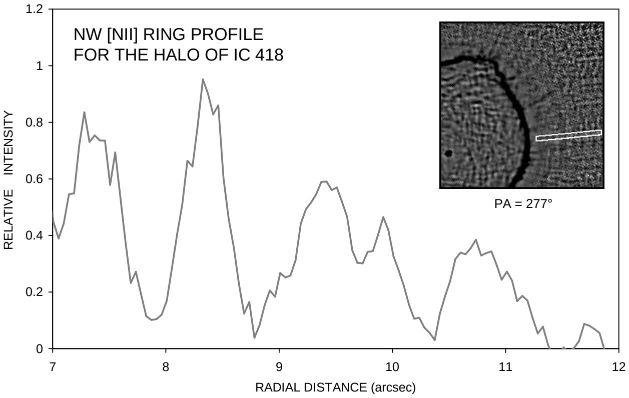

**Figure 4.** Profile through the northwestern region (PA = 277° ) halo ring structures, where the width of the slice is ∼7.3 pixels (≡0.33″). Underlying halo emission has been removed using a fifth-order least-squares polynomial fit.

We note that the model and kinematical age discussed above only applies to the outer skirts of the shell probed by the emission in the low-ionization [N II] line. Higher excitation material exhibits lower expansion velocities, as suggested by the unresolved H$\alpha$ emission line in our echelle observations and more reliably by the unresolved profile of the otherwise narrow [O III] emission line presented by Gesicki, Acker, & Szczerba (1996). Since higher excitation material is closer to the central star, the difference in line profiles reveals a velocity gradient throughout the nebula.

### 3.2 Radial filaments and rings

The *HST* [N II] image and, to some extent, the H$\alpha$ image, disclose a system of radial filaments or rays that emanate from the bright shell of IC 418, as illustrated by the *HST* composite-colour picture shown in Figure 1-*bottom.* These filaments are mostly radial, pointing towards the location of the central star, and their surface brightness is small, $\leqslant$2% the surface brightness peak of the main nebula. Their size is variable, but in a few cases we measure extensions up to 2.″7. We also note the presence of little blisters or "bubble-like" features onto the exterior walls of the bright nebular shell.

A close inspection of the regions just outside the bright ionised shell of IC 418 reveals [N II] and H$\alpha$ emission dis-

**Table 2.** Line ratios comparison for the OSN and OAN observations of IC 418.

| Line ratio | OSN | | OAN | P04 | H00 | H94 | JPP90 | GM85 | A83 | TP80 | K76 |
|---|---|---|---|---|---|---|---|---|---|---|---|
| | W65″ | W105″ | N23″ | | | | 15″ | | | | |
| [O III]$\lambda$5007/H$\alpha$ | 0.69 | 0.52 | 0.44 | 0.36 | 0.43 | 0.24 | 0.32 | 0.53 | 0.53 | 0.46 | 0.49 |
| [N II]$\lambda$6584/H$\alpha$ | 0.41 | 0.67 | 0.63 | 0.64 | 0.61 | 0.59 | 0.66 | 0.53 | 0.57 | 0.59 | 0.61 |

**Notes:** OSN (Observatorio de Sierra Nevada) this paper; OAN (Observatorio Astronómico Nacional) this paper; P04: Pottasch, S.R., et al., (2004); H00: Henry, R.B.C., et al., (2000); H94: Hyung, S., et al., (1994); JPP90: Phillips, J.P., et al. (1990); GM85: Gutiérrez-Moreno, A., et al, (1985); A83: Aller, L.H. & Czyzak S.J., (1983); TP80: Torres-Peimbert, et al., (1980); K76: Kaler, J.B., (1976).

tributed along several elliptical arcs. These are best seen in Figure 3, where we can identify up to three concentric elliptical arcs that enclose the inner shell. Their surface brightness is significantly low, ∼2.5 %, ∼1.4 %, and ∼0.7 % the brightness peak of the inner shell, and their separation can be estimated to be ∼1″. Although these are among the observations with the highest-resolution so far obtained for structures of this kind (see also Balick, Wilson, & Hajian 2001; Corradi et al. 2004), they show the rings to be featureless and relatively broad. A profile through the northwestern region of these structures is shown in Figure 4. The surface-brightness profile is dominated by emission scattered from the bright inner shell that we have subtracted using a fifth-order least-squares polynomial. Figure 4 suggests that the separation between rings is no uniform, with an averaged distance between peaks ∼1″, similar to our previous estimate. This profile even suggests a larger number of rings, but the quality of the observations precludes us to make a more definite statement.

## 3.3 Haloes

### *3.3.1 Inner halo*

After the publication of the analysis of $J-H$ and $H-K_S$ maps of a sample of PNe including IC 418 (Phillips & Ramos-Larios 2005), a close inspection of the *2MASS J*-band image hinted the presence of a round faint halo with radius ≃75″. Since the detection of faint structures around bright nebulae is hindered by instrumental artifacts that produce "ghost haloes" (Corradi et al. 2003), the true nature of this structure remained unclear. The new $JHK$ band images obtained with CAMILA (Figure 5-*top*) find a halo with the same spatial extent as the one hinted in *2MASS* images. The additional *WISE* images unambiguously confirm the presence and spatial extent of this halo that will be referred as the inner halo of IC 418.

This inner halo is basically detected in the $J$ near-IR band and the W1 3.4 $\mu$m *WISE* band (Figure 5-*middle*), with much fainter emission in the $H$ and $K$ near-IR and the W2 *WISE* bands. The nature of this emission is clarified by the near-IR spectrum of the halo of IC 418 described by Hora, Latter, & Deutsch (1999) that shows the H I Pa$\beta$ $\lambda$1.2817 $\mu$m line to be the main contributor to the emission in the $J$ band. Therefore, the inner halo of IC 418 is ionised. There are no mid-IR spectra for the halo, but the *ISO* spectrum of the central region of IC 418 presented by Pottasch et al. (2004) suggests that the *WISE* W1 band may be dominated by the H I 5-4 $\lambda$4.053 $\mu$m line. The lack of continuum emission in the *ISO* spectrum further strengthens our presumption that the emission from this halo comes from ionised material.

### *3.3.2 Outer halo*

The *WISE* images of IC 418 reveal an unexpected additional elliptical shell with its major axis along PA∼300° and a size of 220″×250″(Figure 5-*bottom*). This shell is ∼5 times fainter than the inner halo in the *WISE* W1 band, it has a noticeable limb-brightened morphology, and its Western tip is brighter than the Eastern tip. Given its limb-brightened morphology, we will refer to it as the outer halo of IC 418 (Chu, Jacoby, & Arendt 1987).

The elliptical morphology and asymmetrical brightness distribution of this outer halo may be indicative of the motion of IC 418 relative to the interstellar medium (Tweedy & Kwitter 1996; Villaver, García-Segura, & Manchado 2003; Wareing, Zijlstra, & O'Brien 2007). The off-centered position of the main nebula, shifted by 6″ along the direction pointing towards the apex of the outer halo at PA∼300°, is consistent with this hypothesis.

### *3.3.3* **Spectral properties of the haloes**

High- and intermediate-dispersion long-slit spectroscopic observations of the haloes of IC 418 have been obtained in an effort to determine their kinematical and spectral properties. Unfortunately, no kinematical information is available because the low surface brightness of the haloes has not allowed us to detect their emission in the MES high-dispersion spectroscopic observations, but the OAN and OSN intermediate-dispersion spectroscopic observations have detected the emission from these haloes. The values of the [O III] $\lambda$5007/H$\alpha$ and [N II] $\lambda$6584/H$\alpha$ line ratios derived from these observations are listed in Table 2, together with the values reported by different authors for the central region of IC 418.

A statistical analysis of the different values of the line ratios reported by different authors for the central region of IC 418 yields averaged [O III] $\lambda$5007/H$\alpha$ and [N II] $\lambda$6584/H$\alpha$ line ratios of 0.42±0.10 and 0.60±0.04, respectively. These lines ratios are analogous to those derived from the OAN spectrum offset 23″ North, marginally consistent with those of the OSN spectrum offset 105″ West, and notably different to those of the OSN spectrum offset 65″ West. We note here that the OAN spectrum is too close to the bright central nebula and, as a result, it is considerably contaminated by dispersed light. The OSN spectrum offset $105''$ West is very faint and the line ratios affected by considerable uncertainties. On the other hand, the OSN spectrum offset $65''$ West shows definite different line ratios than the central regions of IC 418 and the spatial distribution of the emission is consistent with the limb-brightened morphology of this halo, proving that the inner halo is indeed ionized and that its excitation is higher than this of the inner regions of IC 418.

## 4 DISCUSSION

IC 418 is a bright and young PN which is optically thick to H-ionising radiation. Such condition may imply the existence of a region of neutral or molecular material outside the main nebula, although conclusive evidence for the occurrence and spatial extent of this region has been lacking. Using narrow-band optical and broad-band near-IR and mid-IR images, and optical long-slit intermediate-dispersion and echelle spectra, we have searched for emission outside the bright inner shell of IC 418. The analysis of these observations has revealed different structures outside the main nebular shell of IC 418: radial rays, rings, blisters and a double system of haloes.

These features are common in many other extended PNe. For instance, the blisters, “bubble-like” features onto the surface of the inner shell can be seen in the Ring Nebula, NGC 6720 (O’Dell et al. 2002) and they reveal that the outer walls of the ionised shells of PNe may be subject of turbulence and instabilities. Meanwhile, the radial filaments (rays in the nomenclature of Balick 2004; Sahai, Morris, & Villar 2011), have been described in many PNe such as NGC 6853 (Hora et al. 2006), NGC 6543 (Balick 2004), or in the mid-IR observations of NGC 40 (Ramos-Larios, Phillips, & Cuesta 2011). The origin of these features has been associated to “ionisation shadows” produced by dense knots and the subsequent ionisation by leaking UV photons (Balick 2004).

The rings around the bright central regions of PNe have been reported for a growing number of PNe (e.g., Corradi et al. 2004; Kwok & Su 2005; Sahai, Morris, & Villar 2011; Ramos-Larios, Phillips, & Cuesta 2011). Their origin and formation are uncertain (see, for instance, Soker 2000; García-Segura, López, & Franco 2001), but they represent radial enhancements in particle density that suggests mass-loss gasping in the late phases of the AGB evolution. At the distance of 1.3 kpc towards IC 418 (Guzmán et al. 2009), the time-lapse between rings would be $\sim 630/(v/10\mathrm{kms}^{-1})$ yr, where a typical expansion velocity of 10 km s$^{-1}$ is assumed for the AGB wind.

The double-halo morphology of IC 418 in the IR is very similar to those found in Cn 1-5, IC 2165, NGC 2022, and NGC 6826 in the optical (Corradi et al. 2003), possibly implying similar formation mechanisms. Corradi et al. (2003) argue that the inner of the two haloes of these PNe is a recombination halo (Redman & Dyson 1999), whereas the outer halo is an AGB halo. This is not probably the case for IC 418, as the ionising flux of its central star has not reached its maximum value yet.

The time-lapse between shells of multiple shell PNe can be compared to the time between thermal pulses at the

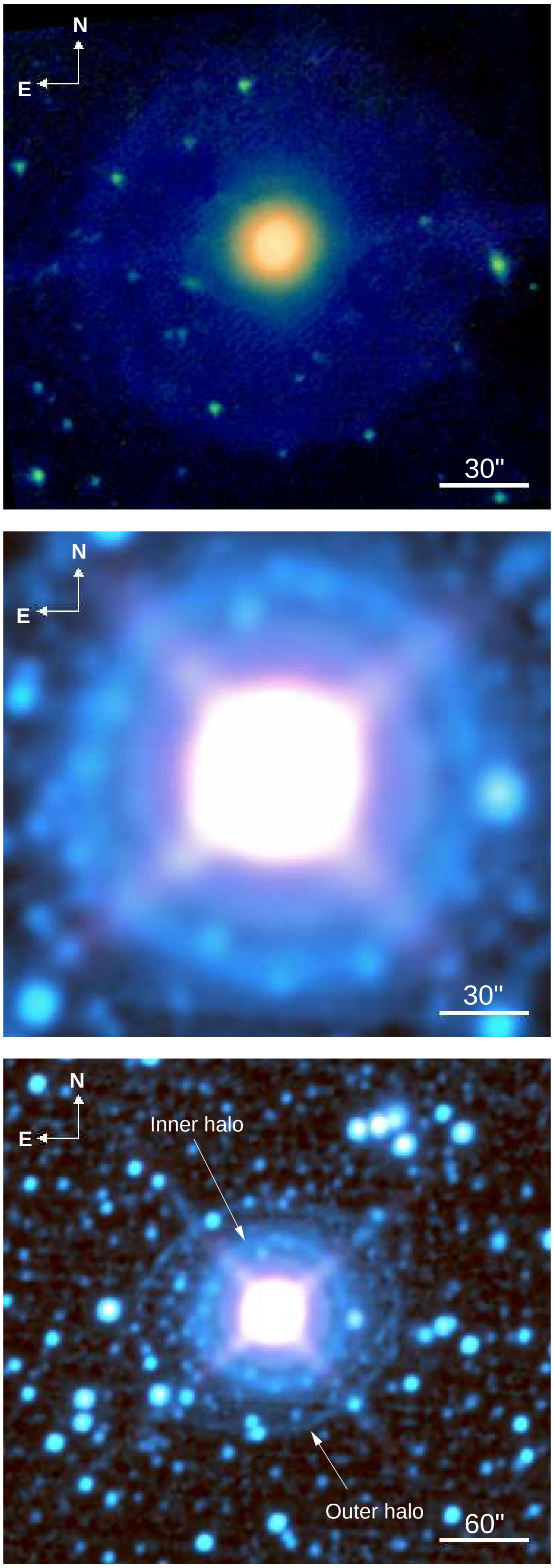

**Figure 5.** (*top*) OAN CAMILA *JHK* and (*middle-bottom*) *WISE* (W1 and W2) composite colour pictures of IC 418. In the *JHK* picture, *J* is blue, *H* is green, and $K'$ is red, while in the *WISE* picture, W1 is blue-green and W2 is red. The *WISE* images have been processed using unsharp masking techniques, leading to the apparent image “sharpening” (Levi 1974).

end of the AGB phase (Vassiliadis & Wood 1993), although hydrodynamical and radiative processes can alter appreciably the kinematics and evolution of the haloes and limit this comparison (Villaver, García-Segura, & Manchado 2002; Villaver, Manchado, & García-Segura 2002; Schönberner & Steffen 2003). At the distance of 1.3 kpc and adopting a typical expansion velocity of 10 km s$^{-1}$, the kinematical ages of the outer and inner halo are $\sim 69,000/(v/10\mathrm{kms}^{-1})$ and $\sim 47,000/(v/10\mathrm{kms}^{-1})$ yr, respectively, whereas the kinematical age of the inner shell was estimated to be $\tau_{\mathrm{kin}} = 2600\,\mathrm{yr}$. The inter-shell time lapses are, thus, $\sim 20,000/(v/10\mathrm{kms}^{-1})$ yr and $\sim 45,000/(v/10\mathrm{kms}^{-1})$ yr. Accounting for the lack of information on the expansion of the haloes of IC 418 and for the very likely dynamical effects that have modified their kinematical age, the mass-loss history of IC 418 can be roughly described to consist of three major episodes of mass-loss separated by 10,000–50,000 yr, with the final one occurring ∼3,000 yr ago after having been preceded by several mass-loss gasps.

In the detection of the faint haloes around IC 418, the near- and mid-IR images have provided especially helpful. Indeed, the generalized use of near- and mid-IR observations of PNe have detected a significant number of faint outer structures around the main nebular shells of many PNe, e.g., MeWe 1-3 and NGC 6852 (Chu et al. 2009), NGC 40 (Ramos-Larios, Phillips, & Cuesta 2011), NGC 3242 and NGC 7354 (Phillips et al. 2009), NGC 1514 (Ressler et al. 2010).

## 5 SUMMARY

We present observations of IC 418 that for the first time probe the presence of different structures around the bright main nebular shell including radial filaments or rays, a system of three concentric rings, and two detached haloes. The outer halo has an elliptical shape and the main nebula is off-centered with respect to this halo.

The inter-shell time laps between the two haloes and the main nebula are derived to be 10,000–50,000 yr, and the time-lapse between the three concentric rings is ∼630 yr for an assumed expansion velocity of 10 km s$^{-1}$. These concentric rings can be associated to several episodes of mass-loss gasps that preceded the final mass-loss event that formed the main nebular shell.

Finally, we note that the progression of the ionisation front through the nebula is not homogeneous, with the development of instabilities at the outer regions of the ionised shell and the formation of radial structures caused by "shadows" to the leaking UV photons.

## ACKNOWLEDGMENTS

GRL acknowledges support from CONACyT and PROMEP (Mexico). MAG and GRL are partially funded by grant AYA2008-01934 of the Spanish Ministerio de Ciencia e Innovación (MICINN) which includes FEDER funds. RV, LO, MAG, and GRL thank support by grant IN109509 (PAPIIT-DGAPA-UNAM). MAG also acknowledges support of the grant AYA 2011-29754-C03-02. Also we want to thank to the OAN-SPM staff and the CATT for time allocation and an anonymous referee who made very useful comments for the improvement of the paper.

Based on observations made with the 2.1m telescope of the Observatorio Astronómico Nacional at the Sierra de San Pedro Mártir (OAN-SPM), which is a national facility operated by the Instituto de Astronomía of the Universidad Nacional Autónoma de México, the Italian Telescopio Nazionale Galileo (TNG) operated on the island of La Palma by the Fundación Galileo Galilei of the INAF (Istituto Nazionale di Astrofisica) at the Spanish Observatorio del Roque de los Muchachos of the Instituto de Astrofísica de Canarias, and the 1.5m telescope at the Observatorio de Sierra Nevada (OSN), Granada, Spain, which is operated by the Instituto de Astrofísica de Andalucía.

This research has made use of the NASA/IPAC Infrared Science Archive, which is operated by the Jet Propulsion Laboratory, California Institute of Technology, under contract with the National Aeronautics and Space Administration. We have also used archival observations made with the NASA/ESA Hubble Space Telescope, and obtained from the Hubble Legacy Archive, which is a collaboration between the Space Telescope Science Institute (STScI/NASA), the Space Telescope European Coordinating Facility (ST-ECF/ESA) and the Canadian Astronomy Data Centre (CADC/NRC/CSA).

We would like to dedicate this paper in memory of our colleague and friend Dr. Yolanda Gómez Castellanos who recently passed away. We would also like to remember Prof. John Peter Phillips whose inspiration provided the motivation for this research although he unfortunately could not see it complete.

## REFERENCES

Aller L. H., Czyzak S. J., 1983, ApJS, 51, 211
Baffa C., et al., 2001, A&A, 378, 722
Balick B., Gonzalez G., Frank A., Jacoby G., 1992, ApJ, 392, 582
Balick B., Wilson J., Hajian A. R., 2001, AJ, 121, 354
Balick B., 2004, AJ, 127, 2262
Chu Y.-H., Jacoby G. H., Arendt R., 1987, ApJS, 64, 529
Chu Y.-H., et al., 2009, AJ, 138, 691
Corradi R. L. M., Schönberner D., Steffen M., Perinotto M., 2003, MNRAS, 340, 417
Corradi R. L. M., Sánchez-Blázquez P., Mellema G., Giammanco C., Schwarz H. E., 2004, A&A, 417, 637
Cruz-González I., et al., 1994, RMxAA, 29, 197
Frank A., van der Veen W. E. C. J., Balick B., 1994, A&A, 282, 554
García-Segura G., López J. A., Franco J., 2001, ApJ, 560, 928
Gesicki K., Acker A., Szczerba R., 1996, A&A, 309, 907
Gussie G. T., Taylor A. R., Dewdney P. E., Roger R. S., 1995, MNRAS, 273, 790
Gutierrez-Moreno A., Cortes G., Moreno H., 1985, PASP, 97, 397
Guzmán L., Loinard L., Gómez Y., Morisset C., 2009, AJ, 138, 46

Hajian A. R., Frank A., Balick B., Terzian Y., 1997, ApJ, 477, 226

Handler G., et al., 1997, A&A, 320, 125

Henry R. B. C., Kwitter K. B., Bates J. A., 2000, ApJ, 531, 928

Hora J. L., Latter W. B., Smith H. A., Marengo M., 2006, ApJ, 652, 426

Hora J. L., Latter W. B., Deutsch L. K., 1999, ApJS, 124, 195

Huggins, P. J., & Manley, S. P. 2005, PASP, 117, 665

Hyung S., Aller L. H., Feibelman W. A., 1994, PASP, 106, 745

Jacob, R., Schönberner, D., Lehmann, H., Zwanzig, A., Sandin, C., Steffen, M., 2012, in IAU Symp. 283, Planetary Nebulae: an Eye to the Future, eds. A. Manchado, L. Stanghellini, & D. Schönberner, in press

Kaler J. B., 1976, ApJS, 31, 517

Kwok S., Su K. Y. L., 2005, ApJ, 635, L49

Levi L., 1974, Computer Graphics and Image Processing, 3, 163

Meaburn J., López J. A., Gutiérrez L., Quiróz F., Murillo J. M., Valdéz J., Pedrayez M., 2003, RMxAA, 39, 185

Meixner M., Skinner C. J., Keto E., Zijlstra A., Hoare M. G., Arens J. F., Jernigan J. G., 1996, A&A, 313, 234

Monk D. J., Barlow M. J., Clegg R. E. S., 1989, IAUS, 131, 197

Monk D. J., Barlow M. J., Clegg R. E. S., 1990, MNRAS, 242, 457

Morisset C., Georgiev L., 2009, A&A, 507, 1517

Morisset C., Szczerba R., García-Hernández, A., García-Lario P., 2012, in IAU Symp. 283, Planetary Nebulae: an Eye to the Future, eds. A. Manchado, L. Stanghellini, & D. Schönberner, in press

O'Dell C. R., Balick B., Hajian A. R., Henney W. J., Burkert A., 2002, AJ, 123, 3329

Olguín L., Vázquez R., Contreras M. E., Jiménez M. Y., 2011, RMxAC, 40, 193

Pauldrach A. W. A., Hoffmann T. L., Méndez R. H., 2004, A&A, 419, 1111

Phillips J. P., Mampaso A., Vílchez J. M., Gomez P., 1986, Ap&SS, 122, 81

Phillips J. P., Riera A., Mampaso A., 1990, Ap&SS, 171, 173

Phillips J. P., Riera A., Mampaso A., 1990, A&A, 234, 454

Phillips J. P., 2003, MNRAS, 344, 501

Phillips J. P., Ramos-Larios G., 2005, MNRAS, 364, 849

Phillips J. P., Ramos-Larios G., Schröder K.-P., Contreras J. L. V., 2009, MNRAS, 399, 1126

Pottasch S. R., Bernard-Salas J., Beintema D. A., Feibelman W. A., 2004, A&A, 423, 593

Prinja R. K., Massa D. L., Urbaneja M. A., Kudritzki R.-P., 2012, arXiv, arXiv:1202.6544

Ramos-Larios G., Phillips J. P., Cuesta L. C., 2011, MNRAS, 411, 1245

Redman M. P., Dyson J. E., 1999, MNRAS, 302, L17

Ressler M. E., Cohen M., Wachter S., Hoard D. W., Mainzer A. K., Wright E. L., 2010, AJ, 140, 1882

Sahai R., Morris M. R., Villar G. G., 2011, AJ, 141, 134

Sahai, R., & Trauger, J. T. 1998, AJ, 116, 1357

Schönberner D., & Steffen M., 2003, IAUS, 209, 147

Shaw R. A., Dufour R. J., 1995, PASP, 107, 896

Soker N., 2000, ApJ, 540, 436

Stanghellini L., Pasquali A., 1995, ApJ, 452, 286

Steffen W., Koning N., Wenger S., Morisset C., Magnor M., 2011, IEEE Transactions on Visualization and Computer Graphics, 17, 454

Taylor A. R., Gussie G. T., Goss W. M., 1989, ApJ, 340, 932

Torres-Peimbert S., Peimbert M., Daltabuit E., 1980, ApJ, 238, 133

Tweedy R. W., Kwitter K. B., 1996, ApJS, 107, 255

Vassiliadis E., & Wood P. R., 1993, ApJ, 413, 641

Villaver E., García-Segura G., Manchado A., 2003, ApJ, 585, L49

Villaver E., García-Segura G., Manchado A., 2002, ApJ, 571, 880

Villaver E., Manchado A., García-Segura G., 2002, ApJ, 581, 1204

Wareing C. J., Zijlstra A. A., O'Brien T. J., 2007, MNRAS, 382, 1233

Wright E. L., et al., 2010, AJ, 140, 1868

Zhang C. Y., Kwok S., 1992, ApJ, 385, 255